Ocean Engineering 248 (2022) 110600

Contents lists available at ScienceDirect

Ocean Engineering

journal homepage: www.elsevier.com/locate/oceaneng

Multi-strategy fusion based on sea state codes for AUV motion control ☆

Junhe Wan [a], Yi Zheng [a], Yanping Li [b], Bo He [c], Hui Li [a], Bin Lv [a], Yinglong Wang [a,*]

[a] Institute of Oceanographic Instrumentation, Qilu University of Technology (Shandong Academy of Sciences), 37 Miaoling Road, Qingdao, China

[b] School of Electrical and Information Engineering, Tianjin University, Tianjin, 300072, China

[c] School of Information Science and Engineering, Ocean University of China, 238 Songling Road, Qingdao, China

ARTICLE INFO

Keywords:
Autonomous underwater vehicle
Active disturbance reject control
Fractional calculus
Multi-strategy fusion

ABSTRACT

The performance of motion controller is worst affected by the ocean currents, waves and other marine environments. Therefore, a multi-strategy fusion method is proposed for AUV motion by considering the characteristics of high nonlinearity, strong coupling, the complex marine environment, and the long-term autonomy. A variety of different control methods are integrated, and the appropriate strategy can be chosen automatically according to AUV running state and the external environment. The hysteresis algorithm is introduced to avoid chattering on account of frequent switching. The simulation and experiment results demonstrate that the excellent performance has been attained, such as overshoot and steady-state error. Furthermore, the multi-strategy fusion method is more suitable for AUV's long-term autonomous task and the complex marine environments. It is easy to realize in engineering and has good robustness on a large scale.

1. Introduction

Autonomous underwater vehicle (AUV) is widely recognized to play an essential role in developing unknown ocean and accomplishing different military missions. AUV motion control is critical to solve these problems, which has continued to receive significant interest. However, it is so challenging to design the controller due to high nonlinearity, strong coupling, the complex marine environment, and the long-term autonomy.

Quite a considerable number of methods are used in AUV motion. PID controller (Jalving, 1994; Khodayari and Balochian, 2015) is the most popular for AUV, which works well at set point. However, it is insufficient to suppress the disturbance of ocean currents and waves. Active disturbance rejection controller (ADRC) is independent of model and can reject disturbance of ocean currents and waves actively (Shen et al., 2016; Li et al., 2019). The fuzzy logic method does not depend on a mathematical model and easily realizes in engineering. Nevertheless, the fuzzy rules and the prior knowledge are fundamental, and it is not easy to achieve high precision control (Bing et al., 2014; Zarkasi et al., 2020). A sliding mode controller has been applied to AUV motion because of its insensitivity to parameters and strong anti-interference, but the chattering is difficult to eliminate (Wang et al., 2020; Liang et al., 2018; Zhang et al., 2018). $H\infty$ controller has better robustness, whereas its design is more complex and needs more experience (Mashhad and Mashhadi, 2016). In conclusion, each of these methods has its advantages, disadvantages and scenarios. The motion of AUV has the characteristics of high nonlinearity and strong coupling. The performance of motion controller is worst affected by the ocean currents, waves and other marine environments. Accordingly, it is extremely difficult for a controller to meet all the above conditions.

The multi-strategy fusion method is proposed for AUV motion by considering the characteristics of high nonlinearity, strong coupling, the complex marine environments, and the long-term autonomy. A variety of different control methods are integrated, and the appropriate strategy can be chosen automatically according to AUV running state and the external environment. The multi-strategy fusion method has the advantages of various control methods to achieve the excellent performance of AUV motion system. It has been widely used in image processing (Luo et al., 2014), automobile (Xu et al., 2014), optimization algorithm (Wei et al., 2018), power system (Kan et al., 2016) and many other fields. The major contributions of this paper are highlighted as follows:

- A multi-strategy fusion method based on sea state codes is proposed for AUV motion under the complex marine environments.

☆ This document is the results of the research project funded by the Natural Science Foundation of Shandong (ZR202102180742), National Development and Reform Commission, China Smart Ocean Major Project (2019-37000-73-03-005308) and Institute of Oceanographic Instrumentation Talent Training Fund Project, China (HYPY202108).

* Corresponding author.
E-mail address: wangly@sdas.org (Y. Wang).

https://doi.org/10.1016/j.oceaneng.2022.110600
Received 21 July 2021; Received in revised form 6 January 2022; Accepted 9 January 2022
Available online 12 February 2022

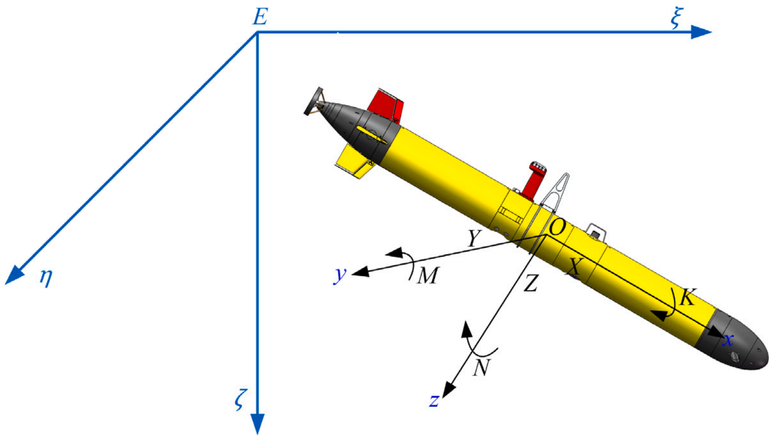

Fig. 1. Earth-fixed and body-fixed reference frames.

Table 1
Notation for AUV in body-fixed reference frame.

Vector	x-axis	y-axis	z-axis
Linear velocity	u	v	ω
Angular velocity	p	q	r
Force	X	Y	Z
Moment	K	M	N

- PID, ADRC, and FOADRC controllers are designed by considering the characteristics of high nonlinearity, strong coupling, the complex marine environments, and the long-term autonomy.
- The hysteresis algorithm is introduced to avoid chattering on account of frequent switching.
- Simulations and experiments demonstrate that the excellent performance has been achieved.

The remainder of this paper is structured as four chapters. Section 2 is devoted to modeling of AUV in 6 DOF, and the transfer function of heading subsystem is derived. Section 3 deals with the controller design based on sea state codes, and the multi-strategy fusion method is proposed. In Section 4, a series of numerical simulations and experiments are presented, and the results are analyzed and discussed in detail. Finally, the key conclusions are drawn in Section 5.

2. Kinematics and dynamic model

2.1. Reference frames

When analyzing the motion of AUV in 6 DOF(degrees of freedom), it is convenient to define two reference frames as illustrated in Fig. 1. The earth-fixed reference frame ($E-\xi\eta\zeta$) has its origin E fixed to the earth. The body-fixed reference frame ($o-xyz$) has its origin O fixed to AUV (Fossen, 2016). Table 1 lists the notations and terms defined by SNAME (Society of Naval Architects and Marine Engineers) and ITTC (International Towing Tank Conference).

2.2. Transformations between body-fixed and earth-fixed

It is assumed that the origin of earth-fixed reference frame E coincides with the origin of body-fixed reference frame O. The earth-fixed reference frame ($E-\xi\eta\zeta$) coincides with the body-fixed reference frame ($o-xyz$) by three principal rotations about the z, y and x axes, as shown in Eq. (1). $E\xi$ and $E\eta$ axes are located in the horizontal plane. $E\xi$ axis rotated 90° clockwise with right-hand rule is $E\eta$ axis. $E\zeta$ axis is perpendicular to $E-\xi\eta\zeta$ plane and points downwards.

$$\begin{bmatrix}\xi\\ \eta\\ \zeta\end{bmatrix}=\begin{bmatrix}cos\psi cos\theta & cos\psi sin\theta sin\varphi - sin\psi cos\varphi & cos\psi sin\theta sin\varphi + sin\psi sin\varphi\\ sin\psi cos\theta & sin\psi sin\theta sin\varphi + cos\psi cos\varphi & sin\psi sin\theta cos\varphi - cos\psi sin\varphi\\ -sin\theta & cos\theta sin\varphi & cos\theta cos\varphi\end{bmatrix}\begin{bmatrix}x\\ y\\ z\end{bmatrix} \tag{1}$$

where ψ represents the heading angle, θ represents the pitch angle, and φ represents the roll angle.

2.3. AUV equations of motion in 6 DOF

The AUV equations of motion in 6 DOF are derived by the Newton–Euler formulation, as shown in Eq. (2). The first three equations present the translational motion, while the last three equations present the rotational motion (Prestero, 2001).

$$\begin{cases} X = m[\dot{u} - vr + wq - x_G(q^2+r^2) + y_G(pq-\dot{r}) \\ \quad +z_G(pr+\dot{q})] \\ Y = m[\dot{v} - wp + ur - y_G(r^2+p^2) + z_G(qr-\dot{p}) \\ \quad +x_G(qp+\dot{r})] \\ Z = m[\dot{w} - uq + vp - z_G(p^2+q^2) + x_G(rp-\dot{q}) \\ \quad +y_G(rq+\dot{p})] \\ K = I_x\dot{q} + (I_x - I_y)qr - (\dot{r}+pq)I_{xz} \\ \quad +(r^2-q^2)I_{yz} + (pr-\dot{q})I_{xy} \\ \quad +m[y_G(\dot{w}-uq+vp) - z_G(\dot{v}-wp+ur)] \\ M = I_y\dot{q} + (I_x - I_z)rp - (\dot{p}+qr)I_{xy} \\ \quad +(p^2-r^2)I_{zx} + (qp-\dot{r})I_{yz} \\ \quad +m[z_G(\dot{u}-vr+wq) - x_G(\dot{w}-uq+up)] \\ N = I_z\dot{r} + (I_y - I_x)pq - (\dot{q}+rp)I_{yz} \\ \quad +(q^2-p^2)I_{xy} + (rq-\dot{p})I_{zx} \\ \quad +m[x_G(\dot{v}-wp+ur) - y_G(\dot{u}-vr+wq)] \end{cases} \tag{2}$$

When the origin of the body-fixed coordinate system coincides with the center of gravity, the AUV equations of motion can reduce to

$$\begin{cases} X = m(\dot{u} - vr + wq) \\ Y = m(\dot{v} - wp + ur) \\ Z = m(\dot{w} - uq + vp) \\ K = I_x\dot{q} + (I_x - I_y)qr \\ M = I_y\dot{q} + (I_x - I_z)rp \\ N = I_z\dot{r} + (I_y - I_x)pq \end{cases} \tag{3}$$

where m: AUV mass;

L: the length of AUV;

x_G, y_G, z_G: coordinates of center of gravity for AUV;

I_x, I_y, I_z: moments of inertia about x, y and z axes;

I_{xy}, I_{yz}, I_{zx}: products of inertia about xoy, yoz and xoz planes.

Substituting the external force (hydrodynamic force, hydrostatic force, rudder force and propulsion force) into Eq. (3) yields the equations of motion in 6 DOF.

Surge equation along the x-axis is described as Eq. (4).

$$\begin{aligned} m(\dot{u}-vr+wq) =& \frac{1}{2}\rho L^4[X'_{qq}q^2+X'_{rr}r^2+X'_{rp}rp] \\ &+\frac{1}{2}\rho L^3[X'_{\dot{u}}\dot{u}+X'_{vr}vr+X'_{wq}wq] \\ &+\frac{1}{2}\rho L^2[X'_{uu}u^2+X'_{vv}v^2+X'_{ww}w^2]+X_{prop} \end{aligned} \tag{4}$$

Sway equation along the y-axis is described as Eq. (5).

$$\begin{aligned} m(\dot{v}-wp+vr) =& \frac{1}{2}\rho L^4[Y'_{\dot{r}}\dot{r}+Y'_{\dot{p}}\dot{p}+Y'_{p|p|}p|p|+Y'_{pq}pq] \\ &+\frac{1}{2}\rho L^3[Y'_{\dot{v}}\dot{v}+Y'_{vq}vq+Y'_{wp}wp+Y'_{wr}wr] \\ &+\frac{1}{2}\rho L^3[Y'_{r}ur+Y'_{p}up+Y'_{v|r|}\frac{v}{|v|}|(v^2+w^2)^{\frac{1}{2}}\,\|\,r|] \\ &+\frac{1}{2}\rho L^2[Y'_{0}u^2+Y'_{v}uv+Y'_{v|v|}|(v^2+w^2)^{\frac{1}{2}}|] \\ &+\frac{1}{2}\rho L^2Y'_{vw}vw+Y_{\delta} \end{aligned} \tag{5}$$

Heave equation along the z-axis is described as Eq. (6).

$$\begin{aligned} m(\dot{w}-uq+vp) =& \frac{1}{2}\rho L^4[Z'_{\dot{q}}\dot{q}+Z'_{pp}p^2+Z'_{rr}r^2+Z'_{rp}rp] \\ &+\frac{1}{2}\rho L^3[Z'_{\dot{w}}\dot{w}+Z'_{vr}vr+Z'_{vp}vp] \\ &+\frac{1}{2}\rho L^3[Z'_{q}uq+Z'_{w|q|}\frac{w}{|w|}|(v^2+w^2)^{\frac{1}{2}}\,\|\,q|] \\ &+\frac{1}{2}\rho L^2[Z'_{0}u^2+Z'_{w}uw+Z'_{w|w|}w|(v^2+w^2)^{\frac{1}{2}}|] \\ &+\frac{1}{2}\rho L^2[Z'_{|w|}u|w|+Z'_{ww}|w(v^2+w^2)^{\frac{1}{2}}|] \\ &+\frac{1}{2}\rho L^2Z'_{vv}v^2+Z_{\delta} \end{aligned} \tag{6}$$

Roll equation about the x-axis is described as Eq. (7).

$$\begin{aligned} I_x\dot{p}+(I_z-I_y)qr =& \frac{1}{2}\rho L^5[K'_{\dot{p}}\dot{p}+K'_{\dot{r}}\dot{r}+K'_{qr}qr+K'_{pq}pq+K'_{p|p|}p|p|] \\ &+\frac{1}{2}\rho L^4[K'_{p}up+K'_{r}ur+K'_{\dot{v}}\dot{v}] \\ &+\frac{1}{2}\rho L^4[K'_{vq}vq+K'_{wp}wp+K'_{wr}wr] \\ &+\frac{1}{2}\rho L^3[K'_{0}u^2+K'_{v}uv+K'_{v|v|}v|(v^2+w^2)^{\frac{1}{2}}|] \\ &+\frac{1}{2}\rho L^3K'_{vw}vw-Whcos\varphi sin\varphi \end{aligned} \tag{7}$$

Pitch equation about the y-axis is described as Eq. (8).

$$\begin{aligned} I_y\dot{q}+(I_x-I_z)rp =& \frac{1}{2}\rho L^5[M'_{\dot{q}}\dot{q}+M'_{pp}p^2+M'_{rr}r^2+M'_{rp}rp+M'_{q|q|}q|q|] \\ &+\frac{1}{2}\rho L^4[M'_{\dot{w}}\dot{w}+M'_{vr}vr+M'_{vp}vp] \\ &+\frac{1}{2}\rho L^4[M'_{q}uq+M'_{|w|q}|(v^2+w^2)^{\frac{1}{2}}q] \\ &+\frac{1}{2}\rho L^3[M'_{0}u^2+M'_{w}uw+M'_{w|w|}w|(v^2+w^2)^{\frac{1}{2}}|] \\ &+\frac{1}{2}\rho L^3[M'_{|w|}u|w|+M'_{ww}|w(v^2+w^2)^{\frac{1}{2}}|] \\ &+\frac{1}{2}\rho L^3M'_{vv}v^2-hW\sin\theta+M_{\delta} \end{aligned} \tag{8}$$

Yaw equation about the z-axis is described as Eq. (9).

$$\begin{aligned} I_z\dot{r}+(I_y-I_x)pq =& \frac{1}{2}\rho L^5[N'_{\dot{r}}\dot{r}+N'_{\dot{p}}\dot{p}+N'_{pq}pq+N'_{qr}qr+N'_{r|r|}r|r|] \\ &+\frac{1}{2}\rho L^4[N'_{wr}wr+N'_{wp}wp+N'_{vq}vq] \\ &+\frac{1}{2}\rho L^4[N'_{p}up+N'_{r}ur+N'_{|v|r}|(v^2+w^2)^{\frac{1}{2}}r] \\ &+\frac{1}{2}\rho L^3[N'_{0}u^2+N'_{v}uv+N'_{v|v|}v|(v^2+w^2)^{\frac{1}{2}}|] \\ &+\frac{1}{2}\rho L^3N'_{vw}vw+N_{\delta} \end{aligned} \tag{9}$$

The acceleration terms are separated from the motion equations of AUV, as shown in Eq. (10) .

$$\begin{bmatrix}\dot{u}\\ \dot{v}\\ \dot{w}\\ \dot{p}\\ \dot{q}\\ \dot{r}\end{bmatrix}=\begin{bmatrix} m-X_{\dot{u}} & 0 & 0 & 0 & 0 & 0\\ 0 & m-Y_{\dot{v}} & 0 & -Y_{\dot{p}} & 0 & -Y_{\dot{r}}\\ 0 & 0 & m-Z_{\dot{w}} & 0 & -Z_{\dot{q}} & 0\\ 0 & -Y_{\dot{p}} & 0 & I_x-K_{\dot{p}} & 0 & -K_{\dot{r}}\\ 0 & 0 & -Z_{\dot{q}} & 0 & I_y-M_{\dot{q}} & 0\\ 0 & -Y_{\dot{r}} & 0 & -K_{\dot{r}} & 0 & I_z-N_{\dot{r}} \end{bmatrix}^{-1}\begin{bmatrix}X\\ Y\\ Z\\ K\\ M\\ N\end{bmatrix} \tag{10}$$

where W is the gravity of AUV, h is the distance between the center of gravity and the center of buoyancy, X_{prop} is the propulsion force, and $Y_{\delta}, Z_{\delta}, M_{\delta}, N_{\delta}$ are the rudder forces and moments.

2.4. AUV equations of motion in the horizontal plane

As described in (11), the horizontal motion of AUV is given by the motion components in surge, sway and yaw. This implies that the motion in heave, roll and pitch are neglected. In addition, it is assumed that AUV has homogeneous mass distribution and xz-plane and xy-plane symmetry (Fossen, 2013).

$$\begin{cases} m(\dot{u}-vr)=X\\ m(\dot{v}+ur)=Y\\ I_z\dot{r}=N \end{cases} \tag{11}$$

The first equation can be neglected under the assumption that AUV moves at constant forward speed (Wan et al., 2018). Because of starboard-port and fore-aft symmetry, $Y_{\dot{r}}=0$ and $N_{\dot{v}}=0$. The linearized maneuvering equations are presented in Eq. (12).

$$\begin{bmatrix}\dot{v}\\ \dot{r}\\ \dot{\psi}\end{bmatrix}=\begin{bmatrix} \frac{Y_v}{m-Y_{\dot{v}}} & \frac{Y_r-mu}{m-Y_{\dot{v}}} & 0\\ \frac{N_v}{I_z-N_{\dot{r}}} & \frac{N_r}{I_z-N_{\dot{r}}} & 0\\ 0 & 1 & 0 \end{bmatrix}\begin{bmatrix}v\\ r\\ \psi\end{bmatrix}+\begin{bmatrix}\frac{Y_{\delta}}{m-Y_{\dot{v}}}\\ \frac{N_{\delta}}{I_z-N_{\dot{r}}}\\ 0\end{bmatrix}\delta \tag{12}$$

where δ is the rudder angle, and Y_v, $Y_{\dot{v}}$, Y_r, N_v, $N_{\dot{r}}$, N_r are the hydrodynamic coefficients.

For the state-space model Eq. (12), the transfer function $G_{\psi}(s)$ becomes Eq. (13) (Junhe et al., 2019). A_1, A_0, B_2, B_1, and B_0 are shown in Eq. (14) and (15).

$$G_{\psi}(s)=\frac{\psi}{\delta_r}=\frac{A_1s+A_0}{B_2s^3+B_1s^2+B_0s} \tag{13}$$

$$\begin{cases} A_1=(m-Y_{\dot{v}})N_{\delta}\\ A_0=Y_{\delta}N_v-N_{\delta}Y_v \end{cases} \tag{14}$$

$$\begin{cases} B_2=(I_z-N_{\dot{r}})(m-Y_{\dot{v}})\\ B_1=-Y_v(I_z-N_{\dot{r}})-N_r(m-Y_{\dot{v}})\\ B_0=N_v(mV-Y_r)+Y_vN_r \end{cases} \tag{15}$$

3. Controller design

The performance of controller is worst affected by ocean currents, waves and other marine environments. It is important to design proper

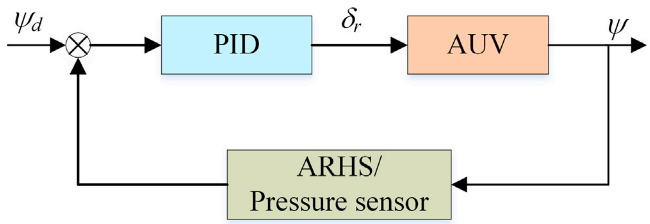

Fig. 2. Schematic diagram of PID controller.

Table 2
Definition of sea state (SS) codes.

Code	Description	Wave height(m)	Percentage probability	
			World wide	North Atlantic
0	Calm	0		
1	Calm	0-0.1	11.2486	8.3103
2	Smooth	0.1–0.5		
3	Slight	0.5–1.25	31.6851	28.1996
4	Moderate	1.25–2.5	40.1944	42.0273
5	Rough	2.5–4.0	12.8005	15.4435
6	Very rough	4.0–6.0	3.0253	4.2938
7	High	6.0–9.0	0.9263	1.4968
8	Very high	9.0–14.0	0.1190	0.2263
9	Phenomenal	Over 14.0	0.0009	0.0016

controllers for different sea state codes. Full details of the definition of sea state codes are given in Fossen (2016). As reported in Table 2, the total probability of the sea state 1, 3 and 4 in the world and North Atlantic are 83.1281% and 78.5372%, respectively. Therefore, we mainly consider the AUV heading subsystem under these three sea states.

3.1. PID controller under sea state 1

The disturbances of ocean currents and wave are slight under sea state 1, so the PID controller is designed for AUV heading. The PID controller is illustrated in Fig. 2 and Eq. (16). The structure of PID is simple and the parameter adjustment is so easy, but the anti-interference ability is poor. Therefore, PID is suitable for sea state 1 with small disturbance.

$$\delta_r(t) = K_p e(t) + K_i \int_0^t e(t) + K_d \frac{de(t)}{dt}, e(t) = \psi_d - \psi \tag{16}$$

where ψ_d is the desired heading, and ψ is the actual heading. K_p is the proportional coefficient, K_i is the integral coefficient and K_d is the differential coefficient.

3.2. ARDC under sea state 3

In view of the sea state 3, an active disturbance rejection controller(ADRC) is designed for AUV heading. The extended state observer of ADRC can effectively estimate the disturbance of signal noise and model uncertainty from the inside of AUV and the disturbance of ocean currents and waves from the outside. ADRC comprises three parts: tracking differentiator (TD), extended state observer (ESO), and nonlinear state error feedback (NLSEF) (Han, 2009), as illustrated in Fig. 3.

Arrange the transient process with respect to desired heading ψ_d. ψ_1 follows the desired heading ψ_d and ψ_2 is the differentiation of ψ_1. According to the heading ψ and the input signal δ_{r0} of AUV, the state ψ_1 is estimated by z_1, the state ψ_2 is estimated by z_2 and the total disturbance acting on AUV is estimated by z_3. δ_{r0} presents the nonlinear state error feedback law (Huang and Xue, 2014; Agee et al., 2015).

$$\begin{cases} \psi_1 = \psi_1 + h\psi_2 \\ \psi_2 = \psi_2 + hfst(\psi_1 - \psi_d, \psi_2, r, h) & TD \\ e = z_1 - \psi \\ \dot{z}_1 = z_2 - \beta_1 e \\ \dot{z}_2 = z_3 - \beta_2 fal(e, 0.5, \varepsilon) + b_0\delta_0 \\ \dot{z}_3 = -\beta_3 fal(e, 0.25, \varepsilon) & ESO \\ e_1 = z_1 - \psi_1, e_2 = z_2 - \psi_2 \\ \delta_{r0} = K_p fal(e, \alpha_1, \varepsilon) + K_d fal(e, \alpha_2, \varepsilon) \\ \delta_r = \delta_{r0} - \frac{z_3}{b_0} & NLSEF \end{cases} \tag{17}$$

where b_0 is the compensation factor, δ_r is the rudder angle, K_p and K_d are the coefficients, and α_1, α_2, β_1, β_2, β_3 are the parameters of ADRC (b_0=0.01, $\alpha_1 = 0.75$, $\alpha_2 = 1.5$, $\beta_1 = 100$, $\beta_2 = 300$, $\beta_3 = 500$, $\varepsilon = 0.0025$).

$$\begin{cases} d = rh \\ d_0 = hd \\ y = e + hx_2 \\ a_0 = \sqrt{d^2 + 8r|y|} \\ a = \begin{cases} x_2 + \frac{a_0 - d}{2} sgn(y), |y| > d_0 \\ x_2 + \frac{y}{h}, |y| \le d_0 \end{cases} \\ fst(e, x_2, r, h) = \begin{cases} -rsgn(a), |a| > d \\ -r\frac{a}{d}, |a| \le d \end{cases} \end{cases} \tag{18}$$

where r is the parameter of controller(r=5) and h is the sampling period(h=0.01).

$$fal(\varepsilon, \gamma, \sigma) = \begin{cases} \frac{\epsilon}{\sigma^{1-\gamma}} |\epsilon| \le \sigma \\ |\epsilon|^\gamma sign(\epsilon)|\epsilon| > \sigma \end{cases} \tag{19}$$

where γ, σ are variable parameters.

3.3. FOADRC under sea state 4

The fractional-order PID has fast dynamic response (Zafer and Karahan, 2012), which can eliminate the estimation error of extended state observer. The fractional-order active disturbance rejection controller (FOADRC) combines the advantages of the fractional-order PID and ADRC, which is designed for higher sea states (Wan et al., 2021). The nonlinear feedback law of ADRC is improved by fractional calculus under sea state 4. The fractional calculus is introduced to obtain zero steady-state error and avoid the oscillation and integral saturation. It will effectively suppress the disturbance of ocean currents and waves. The structure of controller is illustrated in Fig. 4.

Fractional calculus was first proposed by Leibniz (1695). It is an extension of traditional differential and integral to arbitrary (non-integer)

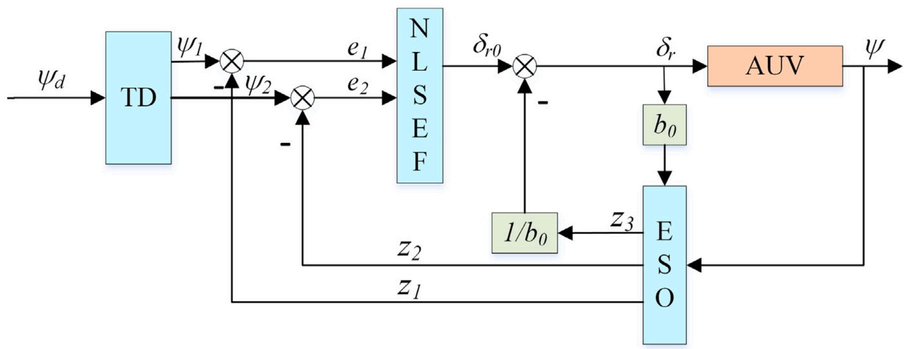

Fig. 3. Schematic diagram of ADR controller.

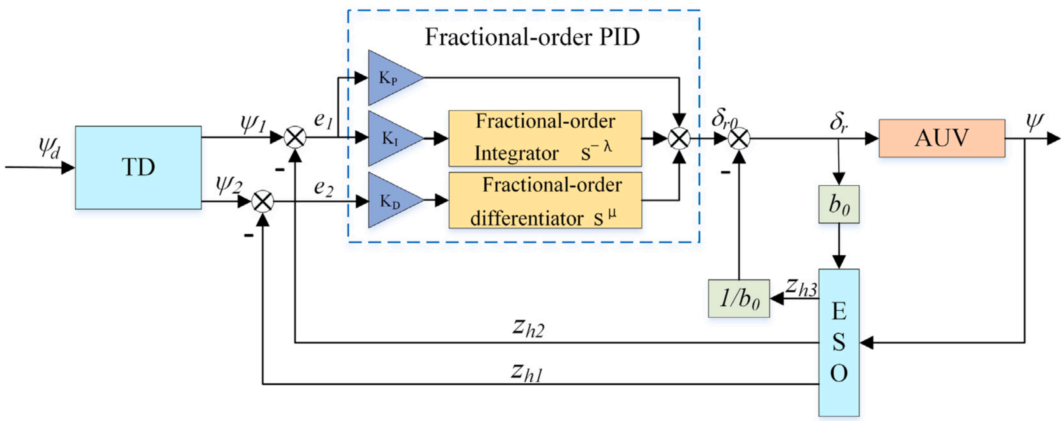

Fig. 4. Schematic diagram of FOADRC.

order (Vilanova and Visioli, 2012; Podlubny, 2002). The Grünwald–Letnikov's definition is illustrated in Eq. (20). Eq. (21) is an approximation of Eq. (20).

$$ {}_a^{GL}\mathcal{D}^{\alpha} f(t) = \lim_{\hat{h}\to 0} \hat{h}^{-\alpha} \sum_{i=0}^{[\frac{t-a}{\hat{h}}]} (-1)^i \binom{a}{i} f(t-i\hat{h}) \tag{20}$$

$$ \mathcal{D}^{\alpha} f(t) \approx \mathcal{D}^{\alpha} f(t) \approx \hat{h}^{-\alpha} \sum_{i=0}^{N(t)} \omega_i^{\alpha} f(t-i\hat{h}) \tag{21}$$

$$ \omega_i^{\alpha} = (-1)^i \binom{a}{i} \tag{22}$$

$$ \omega_0^{\alpha} = 1; \omega_i^{\alpha} = (1 - \frac{\alpha+1}{i})\omega_{i-1}^{\alpha} (i = 1, 2, \dots) \tag{23}$$

Where $\hat{h}$ is the step size, $[\frac{t-a}{\hat{h}}]$ represents the integer part of $[\frac{t-a}{\hat{h}}]$, $\alpha > 0$ is the differential orders and $\alpha < 0$ is the integral and $(|\alpha| \in (0,1))$.

The nonlinear state error feedback law is improved by introducing fractional calculus, and FOADRC is depicted in the following form (Huang et al., 2020; Shi et al., 2018).

$$\begin{cases} \psi_1 = \psi_1 + h\psi_2 & \\ \psi_2 = \psi_2 + hfst(\psi_1 - \psi_d, \psi_2, r, h) & TD \\ e = z_1 - \psi & \\ \dot{z}_1 = z_2 - \beta_1 e & \\ \dot{z}_2 = z_3 - \beta_2 fal(e, 0.5, \varepsilon) + b_0\delta_0 & \\ \dot{z}_3 = -\beta_3 fal(e, 0.25, \varepsilon) & ESO \\ e_1 = z_1 - \psi_1, e_2 = z_2 - \psi_2 & \\ \delta_{r0} = K_{fp}e_1 + K_{fi}\mathcal{D}^{-\lambda}e_1 + K_{fd}\mathcal{D}^{\mu}e_2 & \\ \delta_r = \delta_{r0} - \frac{z_3}{b_0} & NLSEF \end{cases} \tag{24}$$

where K_{fp} is the proportional coefficient of heading angle, K_{fi} is the integral coefficient and K_{fd} is the differential coefficient, λ and μ are the integral and differential orders respectively.

3.4. Multi-strategy fusion based on sea state codes

The controllers can match the sea state codes with good accuracy. PID is adopted for the heading subsystem under sea state 1. However, PID is obviously hard to satisfy the control objective under sea state 3, which switches to ADRC autonomously. Similarly, ADRC switches to fractional-order ADRC under sea state 4 autonomously (see Fig. 5).

3.5. Hysteresis-based switching

The appropriate strategy is selected autonomously according to the sea state codes and the objective function. In order to avoid chattering on account of frequent switching, the hysteresis switching algorithm is introduced for multi-strategy fusion (Hespanha et al., 2003). The objective function is depicted in Eq. (26).

$$ e_i(t) = \psi_d(t) - \psi_i(t) \tag{25}$$

$$ J_i(t) = \alpha e_i^2(t) + \beta \sum_{j=t-l+1}^{t-1} \exp[-\tau(t-j)e_i^2(j)] \tag{26}$$

where $\psi_d(t)$ is the input of system (desired heading), $\psi_i(t)$ is output of controller i at sampling time t, $e_i(t)$ is the error of system, $\alpha \ge 0$, $\beta \ge 0$ are the weightings of errors, and $\tau \ge 0$ is the forgetting factor.

The controller p is working at a certain time t. Let $q = arg\min_{i\in\{1,2\dots m\}} J_i(t), p \ne q$. $J_p(t)$ is not the minimum. If $J_p(t)$ is smaller than $J_q(t) + \rho$, no switching occurs. If $J_p(t)$ is no smaller than $J_q(t) + \rho$, in which case switches to controller q. ρ is a hysteresis constant (Niu

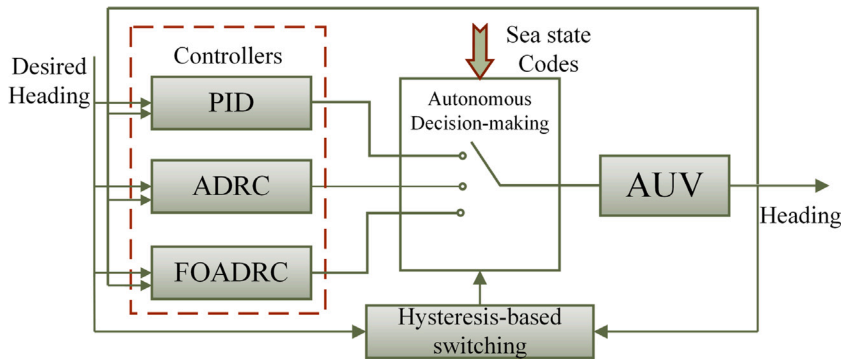

Fig. 5. Schematic diagram Heading system of multi-strategy fusion.

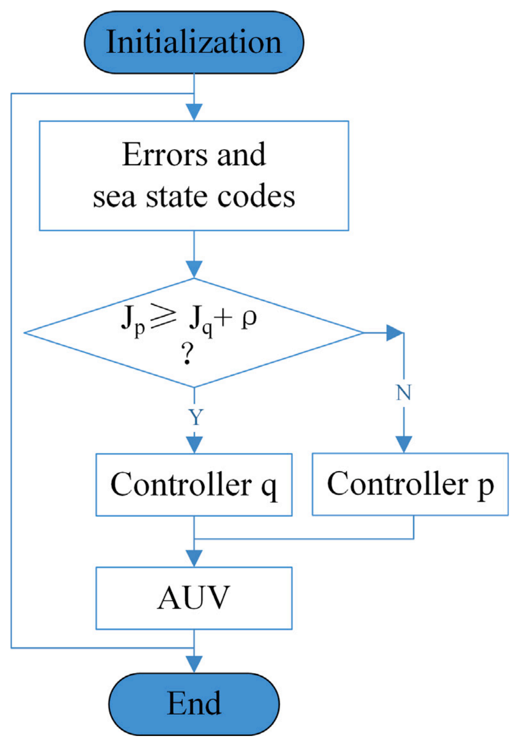

Fig. 6. Flow diagram of hysteresis-based switching.

et al., 2017). The controllers do not switch every time $J_p(t)$ becomes greater than $J_q(t)$, but switch only when $J_p(t)$ becomes *significantly* greater($J_p(t) \geq J_q(t) + \rho$). The chatting will be avoided with the help of hysteresis switching. The flow diagram of hysteresis-based switching is given in Fig. 6.

3.6. Stability of switching system

Consider the continuous-time system Eq. (12) defined on some state space. Eq. (12) can be rewritten as Eq. (27) without loss of generality.

$$\dot{x} = A_{\sigma_{x(t)}} x + B_{\sigma_{x(t)}} u, x \in \mathbb{R}^n, u \in \mathbb{R}^m$$
$$u = K_{\sigma_{x(t)}} x \tag{27}$$

where $A_{\sigma_{x(t)}}, B_{\sigma_{x(t)}}$ are the matrixes with the fixed dimensions, $u = K_{\sigma_{x(t)}} x$ is the state feedback law. $\sigma_{x(t)}$: $R^n \times [0, \infty) \mapsto \mathcal{P} = \{1, 2, \dots p\}$ is the switching function of system and is continuous from the right everywhere. It is a piecewise constant function which depends on the time t or the state $x(t)$. When $\sigma_{x(t)} = j, j \in \mathcal{P}$, the corresponding subsystem becomes active at time t. Suppose that $\mathcal{P} = \{1, 2\}$. The system (Eq. (27)) switches between these two subsystems.

Theorem 1. *Let Eq. (27) be a finite family of globally asymptotically stable systems. Suppose that $(A_{\sigma_{x(t)}}, B_{\sigma_{x(t)}})$ is a controllable pair, there exists two matrixes K_1 and K_2, two real numbers v_1 and v_2, and positive definite matrixes P_1 and P_2 which satisfy inequalities Eq. (28) and (29).*

$$-P_1\bar{A}_1 - \bar{A}_1^T P_1 - 2\lambda_{max}(P_1)I + v_1(P_2 - P_1) > 0 \tag{28}$$
$$-P_2\bar{A}_2 - \bar{A}_2^T P_2 - 2\lambda_{max}(P_2)I + v_2(P_1 - P_2) > 0 \tag{29}$$

where $\bar{A}_j := A_j + B_j K_j$, $\tau_1\tau_2 \geq 0$, and $\lambda_{max}(\cdot)$ denotes the largest eigenvalue of a symmetric matrix.

Then the switch system is asymptotically stable.

Proof. Assume that v_1, v_2 are nonnegative. A Lyapunov function candidate for this system is shown in Eq. (30). A stabilizing switching signal $\sigma_{x(t)}$ is defined by Eq. (31).

$$V_j(x(t)) = x^T P_j x \tag{30}$$
$$\sigma_{x(t)} = argmax V_j(x(t)), j = 1, 2 \tag{31}$$

If $x^T(P_1 - P_2)x \geq 0$ and $x \neq 0$, such that $x^T[P_1\bar{A}_1 + \bar{A}_1^T P_1 + 2\lambda_{max}(P_1)I]x < 0$.

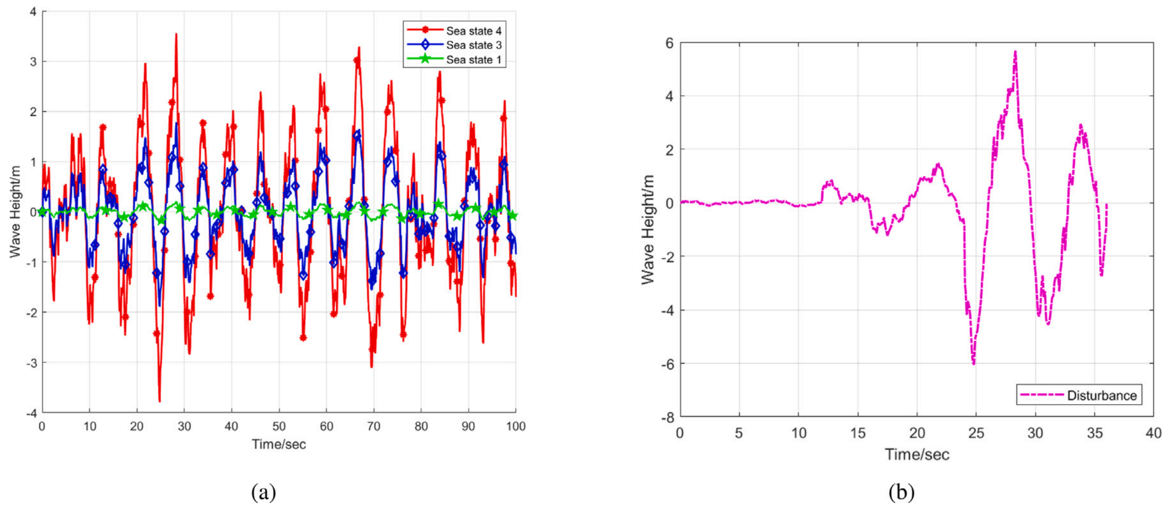

Fig. 7. (a) is the comparisons of three sea states, and (b) is the variation of sea state codes with time.

If $x^T(P_2 - P_1)x \geq 0$ and $x \neq 0$, such that $x^T[P_2\bar{A}_2 + \bar{A}_2^T P_2 + 2\lambda_{max}(P_2)I]x < 0$.

Σ_1 and Σ_2 are written as Eq. (32).

$$\Sigma_1 = \{x \in R^n | x^T(P_1 - P_2)x \geq 0\}, \Sigma_2 = \{x \in R^n | x^T(P_2 - P_1)x \geq 0\} \quad (32)$$

If $\Sigma_1 \bigcup \Sigma_2 = R^n/\{0\}$ and $x \in \Sigma_1$, then for the system Eq. (27) we have

$$\begin{aligned} \dot{V}_1(x(t)) &= \dot{x}^T P_1 x + x^T P_1 x \\ &= [(A_1 + B_1 K_1)x]^T P_1 x + x^T P_1(A_1 + B_1 K_1)x \\ &= x^T(A_1 + B_1 K_1)^T P_1 x + x^T P_1(A_1 + B_1 K_1)x \\ &= x^T[\bar{A}_1^T P_1 + P_1\bar{A}_1]x \\ &\leq x^T[\bar{A}_1^T P_1 + P_1\bar{A}_1 + 2\lambda_{max} P_1 I]x \\ &< 0 \end{aligned} \quad (33)$$

If $x \in \Sigma_2 - \Sigma_1$, time differentiation of $\dot{V}_2(x(t))$ yields

$$\begin{aligned} \dot{V}_2(x(t)) &= \dot{x}^T P_2 x + x^T P_2 x \\ &= [(A_2 + B_2 K_2)x]^T P_2 x + x^T P_2(A_2 + B_2 K_2)x \\ &= x^T(A_2 + B_2 K_2)^T P_2 x + x^T P_2(A_2 + B_2 K_2)x \\ &= x^T[\bar{A}_2^T P_2 + P_2\bar{A}_2]x \\ &\leq x^T[\bar{A}_2^T P_2 + P_2\bar{A}_2 + 2\lambda_{max} P_2 I]x \\ &< 0 \end{aligned} \quad (34)$$

At switching time t_j, we obtain

$$V_{\sigma_{x(t_j)}}(x(t_j)) \leq \lim_{t \to t_j^-} V_{\sigma_{x(t)}}(x(t)) \quad (35)$$

According to multiple Lyapunov functions method (Niu et al., 2020; Fan and Zhu, 2021), the closed-loop switched system Eq. (27) is asymptotically stable.

4. Experiment results and analysis

The simulations and experiments have been conducted to evaluate the performance of controllers under different sea states and the availability of multi-strategy fusion method. A more detailed analysis is presented in the following sections.

4.1. Simulations

4.1.1. Simulations of sea state

According to the definition of sea state codes, the simulations of sea state are illustrated in Fig. 7(a). As shown in Fig. 7(a), the significant wave height is $1.5m - 2.5m$ (red) under sea state 4, the significant wave height is $0.5m - 1.25m$ (blue) under sea state 3, and the significant wave height is $0 - 0.1m$ (green) under sea state 1. As shown in Fig. 7(b), it is sea state 1 from $0s$ to $12s$, it is sea state 3 from $12s$ to $24s$, and it is sea state 4 from $24s$ to $36s$.

Table 3
Steady-State Error of PID, ADRC and FOADRC under three sea states (Unit: °)

Method	Step	Sea state 1	Sea state3	Sea state 4
PID	0	0.28	2.23	4.46
ADRC	0	0.11	0.91	1.82
FOADRC	0	0.098	0.32	0.63

Table 4
Response time of PID, ADRC and FOADRC under three sea states(Unit: s)

Method	Step	Sea state 1	Sea state3	Sea state 4
PID	10	10	10	10
ADRC	10	10	10	10
FOADRC	6	6	6	6

4.1.2. Simulations of controller

The performance of controllers under different sea state codes will be analyzed in detail. Tables 3–5 reports the results of these three controllers under sea state 1, 3 and 4.

Scenario 1: the comparisons in the absence of disturbance

The results are illustrated in Fig. 8(a). The rise time of PID is longer than ADRC and FOADRC, whereas the steady-state errors of these three controllers are zero. They all can meet control requirements.

Scenario 2: the comparisons under sea state 1

The results are illustrated in Fig. 8(b). The steady-state error of PID is 0.28°, and the relative error is 3.5%. The PID controller is within acceptable error range, which is applied for AUV heading subsystem under sea state 1.

Scenario 3: the comparisons under sea state 3

The results are shown in Fig. 8(c). The steady-state error of PID control is increased to 2.23°, and the relative error is 27.8%. The performance gets worse obviously. However, the steady-state error of ADRC is less than half of that of PID, and the control effect is ideal.

Scenario 4: the comparisons under sea state 4

The results are shown in Fig. 8(d). The steady-state error of ADRC is three times of that of fractional-order ADRC, and the performance of ADRC is not satisfactory. Therefore, FOADRC is applied for AUV heading subsystem under sea state 4.

Scenario 5: the comparisons of a strategy and multi-strategy fusion

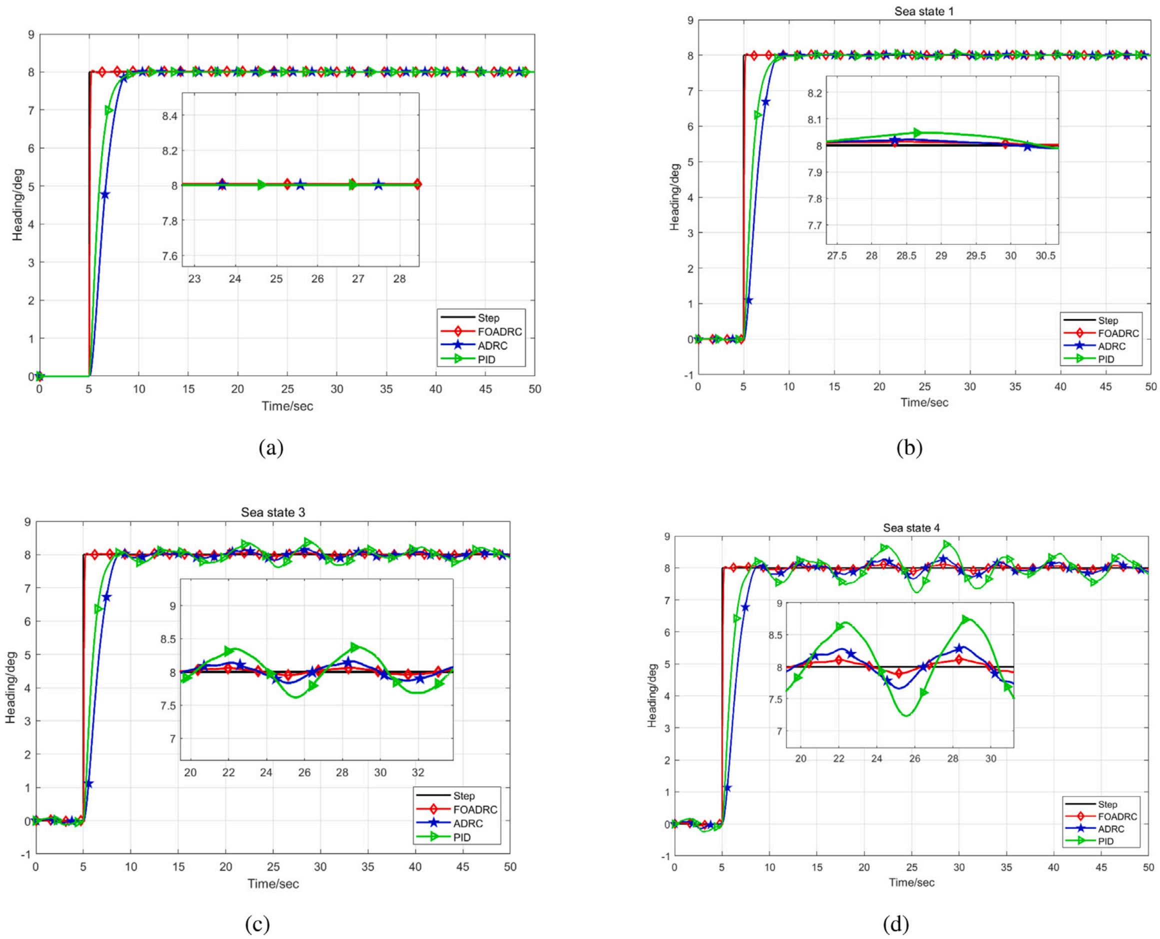

Fig. 8. (a) is the comparison result of controllers in absence of disturbance, (b)is the comparison result under sea state 1, (c) is the comparison result under sea state 3, and (d) is the comparison result under sea state 4.

Table 5
Overshoot of PID, ADRC and FOADRC under three sea states.

Method	Step	Sea state 1	Sea state3	Sea state 4
PID	0	0	1.25%	2.8%
ADRC	0	0	1%	1%
FOADRC	0.6%	0.6%	0.6%	0.63

Table 6
Switching results under sea state 3(Unit: °)

Method	Max	Min	RMS	RMSE	SSE
PID	297.83	292.67	295.69	4.46	4.30
ADRC	298.76	293.63	297.00	3.12	3.00

It is assumed that AUV works for a long time and the sea state gradually worsens. The performance of controllers under three kinds of sea states is reported in Fig. 8(a). Clearly, the performance of PID gets worse with the deterioration of sea state. It is necessary to switch to a controller with stronger anti-interference. The simulation of multi-strategy fusion is reported in Fig. 9(b). Its performance is better than PID and ADRC, and it is more simple than FOADRC. Consequently, the multi-strategy method is superior to a single control strategy. Combining the advantages of several controllers, we construct a strong robust control system under complex marine environment which can meet the most operating environments of AUV.

4.2. Experiments

The multi-strategy fusion method is validated on the $Sailfish$ AUV, as shown in Fig. 10. It is a torpedo-shape AUV with a displacement of 210 Kg, a length of 320cm and a diameter of 32.4cm. It is equipped with AHRS(Attitude and Heading Reference System), DVL(Doppler Velocity Log), GPS(Global Positioning System), SONAR(Sound Navigation and Ranging) and so on.

Scenario 1: PID switches to ADRC under the sea state 3. The desired heading is 300° and the cruise speed is 1.5 m/s.

As shown in Fig. 11, plotting all records yields a curve for the change of heading angle under the sea state 3. Table 6 lists the maximum, minimum, root mean square value(RMS), root mean square error(RMSE) and steady-state error(SSE) of these two controllers. The green solid line with triangles denotes PID, and the blue solid line with stars denotes ADRC. The RMSE and RMS of PID are 4.46° and 295.69°, respectively. The heading fluctuates between 292.67° and 297.83°. When PID switches to ADRC, the steady-state error is reduced by 30.2%. The RMS value 297.00° is closer to the desired heading of 300°. The performance is improved obviously after switching.

Scenario 2: ADRC switches to FOADRC under the sea state 4. The desired heading is 300° and the cruise speed is 1.5 m/s.

As illustrated in Fig. 12, plotting all records yields a curve for the change of heading angle under the sea state 4. Table 7 lists the maximum, minimum, RMS, RMSE and steady state errors of these two controllers. The blue solid line with stars represents ADRC, and the red solid line with diamonds represents FOADRC. It can be seen from the table that the RMS, RMSE and steady-state error of ADRC from 1860s to 1900s are 290.1776°, 10.6272°, 9.8224°, respectively, and the heading

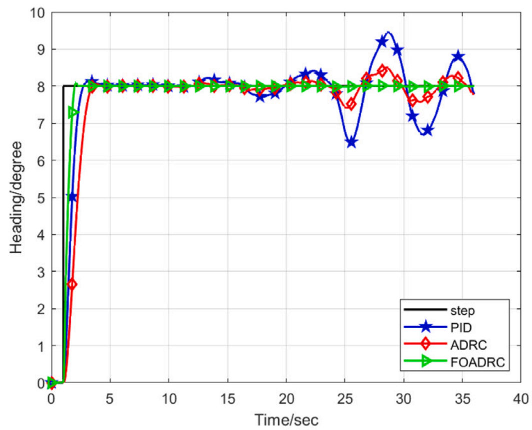

(a)

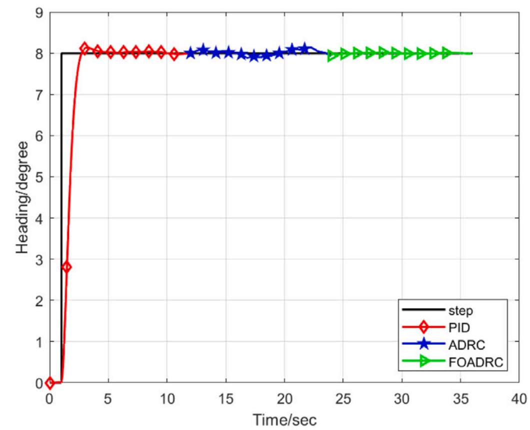

(b)

Fig. 9. (a) is the comparisons of three sea states, and (b) is the variation of sea state codes with time.

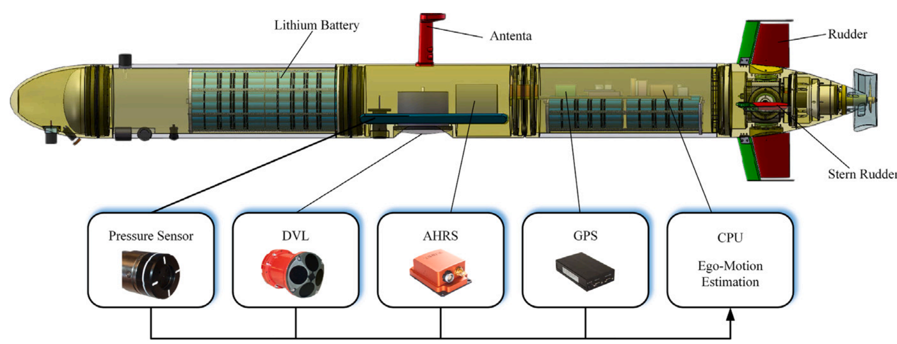

(a)

(b)

Fig. 10. (a) is the structure diagram of AUV, and (b) is the photo of *Sailfish* AUV.

Table 7
Switching results under sea state 4(Unit: °)

Method	Max	Min	RMS	RMSE	SSE
ADRC	297.6	285.1	290.18	10.63	9.82
FOADRC	299.6	292.5	295.70	4.52	4.30

fluctuates between 297.7° and 285.1°. The actual value deviates from the desired heading greatly, and the performance of ADRC is poor. However, the satisfactory performance has been achieved. The RMS error is reduced by 57.5%, steady-state error is reduced by 56.1%, and RMS value 295.70° is closer to the desired heading 300°. The experiments indicate that the performance of multi-strategy fusion method is superior to a single method.

5. Conclusion

This paper proposes a multi-strategy fusion method based on sea state codes for AUV heading subsystem. Firstly, We deduce the equations of motion in 6 DOF and the transfer function of $sailfish$ AUV heading subsystem. Secondly, PID, ADRC and FOADRC controllers are designed based on different sea state codes, and the appropriate strategy is selected autonomously according to the sea state codes and the objective function. Thirdly, the hysteresis algorithm is introduced in order to avoid chattering on account of frequent switching. The stability of the proposed method is proven by multiple Lyapunov functions. Finally, the simulation and experiment results show that the multi-strategy fusion method proposed in this paper is more suitable for AUV's long-term autonomous task and the complex marine

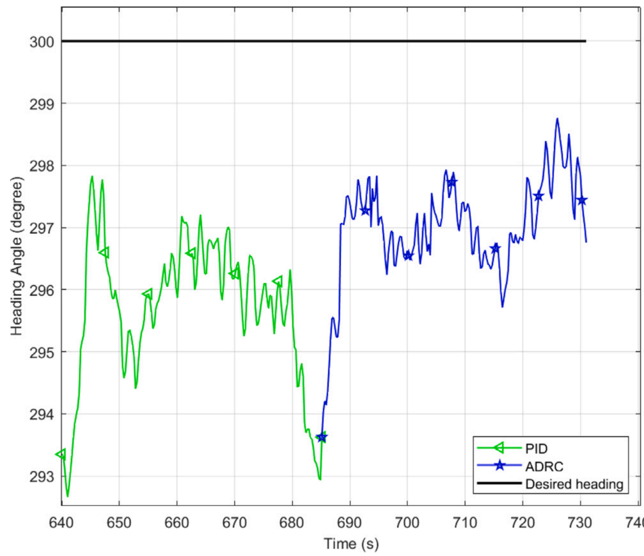

Fig. 11. Switching under sea state 3.

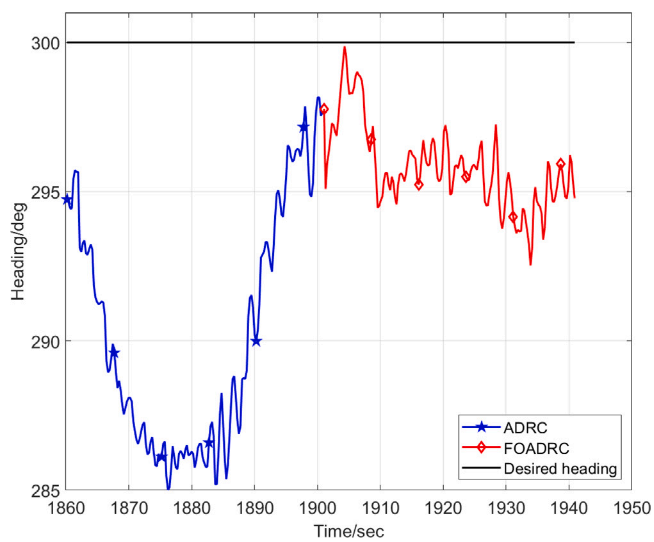

Fig. 12. Switching under sea state 4.

environments. Compared with the single control method, the superior performance has been attained.

In the future, we will apple the optimization algorithm to adjust the control parameters automatically and take more complex marine environments into consideration.

CRediT authorship contribution statement

Junhe Wan: Conceptualization of this study, Methodology, Writing – original draft. **Yi Zheng:** Conceptualization of this study, Methodology. **Yanping Li:** Data curation, Writing – original draft. **Bo He:** Data curation, Validation. **Hui Li:** Software, Writing – review & editing. **Bin Lv:** Validation. **Yinglong Wang:** Conceptualization of this study, Methodology.

Declaration of competing interest

The authors declare that they have no known competing financial interests or personal relationships that could have appeared to influence the work reported in this paper.

Appendix

AUV	Autonomous Underwater Vehicle
PID	Proportional Integral Derivative
ADRC	Active Disturbance Rejection Control
FOADRC	fractional-order active disturbance rejection control
RMS	root mean square
RMSE	root mean square error
SSE	steady-state error

References

Agee, J.T., Bingul, Z., Kizir, S., 2015. Higher-order differential feedback control of a flexible-joint manipulator. J. Vib. Control 21 (10), 1976–1986. http://dx.doi.org/10.1177/1077546313504979.

Bing, S., Zhu, D., Jiang, L., Yang, S.X., 2014. A novel fuzzy control algorithm for three-dimensional AUV path planning based on sonar model. J. Intell. Fuzzy Syst. 26 (6), 2913–2926. http://dx.doi.org/10.3233/IFS-130957.

Fan, L., Zhu, Q., 2021. P th moment exponential stability of switched discrete time stochastic systems: A multiple Lyapunov functions method. J. Franklin Inst. (2), http://dx.doi.org/10.1016/j.jfranklin.2021.07.014.

Fossen, T.I., 2013. Mathematical Models of Ships and Underwater Vehicles. Springer London, London, pp. 1–9. http://dx.doi.org/10.1007/978-1-4471-5102-9_121-2.

Fossen, T.I., 2016. Handbook Of Marine Craft Hydrodynamics And Motion Control. John Wiley & Sons, Ltd, http://dx.doi.org/10.1002/9781119994138.

Han, J., 2009. From PID to active disturbance rejection control. IEEE Trans. Ind. Electron. 56 (3), 900–906. http://dx.doi.org/10.1109/TIE.2008.2011621.

Hespanha, J.P., Liberzon, D., Morse, A.S., 2003. Hysteresis-based supervisory control of uncertain linear systems. Automatica 39 (2), 263–272. http://dx.doi.org/10.1016/S0005-1098(02)00241-8.

Huang, J., Ma, P., Bao, G., et al., 2020. Research on position servo system based on fractional-order extended state observer. IEEE Access PP (99), 1. http://dx.doi.org/10.1109/ACCESS.2020.2997407.

Huang, Y., Xue, W., 2014. Active disturbance rejection control: Methodology and theoretical analysis. Isa. Trans. 53 (4), 963–976. http://dx.doi.org/10.1016/j.isatra.2014.03.003.

Jalving, B., 1994. The NDRE-AUV flight control system. IEEE J. Ocean. Eng. 19 (4), 497–501. http://dx.doi.org/10.1109/48.338385.

Junhe, W., Bo, H., Dianrui, W., et al., 2019. Fractional-order PID motion control for AUV using cloud-model-based quantum genetic algorithm. IEEE Access 7 (99), 124828–124843. http://dx.doi.org/10.1109/ACCESS.2019.2937978.

Kan, L., Sun, K., Xi, J., He, L., 2016. Multi-mode control strategy for primary-side regulation system. In: 2016 13th IEEE International Conference On Solid-State And Integrated Circuit Technology. ICSICT.

Khodayari, M.H., Balochian, S., 2015. Modeling and control of autonomous underwater vehicle (AUV) in heading and depth attitude via self-adaptive fuzzy PID controller. J. Mar. Ence Technol. 20 (3), 559–578. http://dx.doi.org/10.1007/s00773-015-0312-7.

Li, H., He, B., Yin, Q., Mu, X., Zhang, J., Wan, J., Wang, D., Shen, Y., 2019. Fuzzy optimized MFAC based on ADRC in AUV heading control. Electronics 8 (6), 1–32. http://dx.doi.org/10.3390/electronics8060608.

Liang, X., Qu, X., Wan, L., Ma, Q., 2018. Three-dimensional path following of an underactuated AUV based on fuzzy backstepping sliding mode control. Int. J. Fuzzy Syst. 640–649. http://dx.doi.org/10.1007/s40815-017-0386-y.

Luo, X.Q., Zhang, Z.C., Wu, X.J., 2014. Adaptive multistrategy image fusion method. J. Electron. Imag. 23 (5), 053011. http://dx.doi.org/10.1117/1.JEI.23.5.053011.

Mashhad, A.M., Mashhadi, S.K.M., 2016. H infinity robust controller comparison with PD like fuzzy logic controller for an AUV control. In: Iranian Joint Congress On Fuzzy & Intelligent Systems. http://dx.doi.org/10.1109/CFIS.2015.7391665.

Niu, B., Fu, J., Li, T.-F., 2017. Hysteresis-based switching design for stabilization of switched linear neutral systems. Circuits Syst. Signal Process. Cssp http://dx.doi.org/10.1007/s00034-016-0294-7.

Niu, B., Liu, Y., Zhou, W., Li, H., Duan, P., Li, J., 2020. Multiple Lyapunov functions for adaptive neural tracking control of switched nonlinear nonlower-triangular systems. IEEE Trans. Cybern. 1877–1886. http://dx.doi.org/10.1109/TCYB.2019.2906372.

Podlubny, I., 2002. Geometric and physical interpretation of fractional integration and fractional differentiation. Fract. Calc. Appl. Anal. 5 (4), 367–386. http://dx.doi.org/10.1016/j.sigpro.2014.05.026, Dedicated to the 60th anniversary of Prof. Francesco Mainardi.

Prestero, T., 2001. Development of a six-degree of freedom simulation model for the REMUS autonomous underwater vehicle. In: MTS/IEEE Oceans 2001. An Ocean Odyssey. Conference Proceedings (IEEE Cat. No.01CH37295). http://dx.doi.org/10.1109/oceans.2001.968766.

Shen, Y., Shao, K., Ren, W., et al., 2016. Diving control of autonomous underwater vehicle based on improved active disturbance rejection control approach. Neurocomputing 173 (JAN.15PT.3), 1377–1385. http://dx.doi.org/10.1016/j.neucom.2015.09.010.

Shi, X., Chen, Y., Huang, J., 2018. Application of fractional-order active disturbance rejection controller on linear motion system. Control Eng. Pract. 81 (DEC.), 207–214. http://dx.doi.org/10.1016/j.conengprac.2018.09.014.

Vilanova, R., Visioli, A., 2012. PID Control In The Third Millennium. Springer London, http://dx.doi.org/10.1007/978-1-4471-2425-2.

Wan, J., He, B., Shen, Y., 2018. Heading multi-mode control based on soft-switching for autonomous underwater vehicle. Ocean Eng. 164, 672–682. http://dx.doi.org/10.1016/j.oceaneng.2018.06.068.

Wan, J., Liu, H., Yuan, J., Shen, Y., Zhang, H., Wang, H., Zheng, Y., 2021. Motion control of autonomous underwater vehicle based on fractional calculus active disturbance rejection. J. Mar. Sci. Eng. 9 (11), http://dx.doi.org/10.3390/jmse9111306.

Wang, J., Wang, C., Wei, Y., Zhang, C., 2020. Sliding mode based neural adaptive formation control of underactuated AUVs with leader-follower strategy. Appl. Ocean Res. 94, 101971. http://dx.doi.org/10.1016/j.apor.2019.101971.

Wei, F., Yue, M., Zheng, J., 2018. Improved artificial bee colony algorithm based on multi-strategy fusion. Comput. Eng. Appl. 111–116.

Xu, L., Li, J., Ouyang, M., Hna, J., Yang, G., 2014. Multi-mode control strategy for fuel cell electric vehicles regarding fuel economy and durability. Int. J. Hydrogen Energy 39 (5), 2374–2389. http://dx.doi.org/10.1016/j.ijhydene.2013.11.133.

Zafer, B., Karahan, O., 2012. Fractional PID controllers tuned by evolutionary algorithms for robot trajectory control. Turkish J. Electr. Eng. Comput. Sci. 20 (Sup.1), 1123–1136. http://dx.doi.org/10.3906/elk-1102-1011.

Zarkasi, A., Angkotasan, I.J., Ravi, M.A., Yudi, E.D., 2020. Design heading control for steering AUV with fuzzy logic. In: Sriwijaya International Conference On Information Technology And Its Applications. SICONIAN 2019, http://dx.doi.org/10.2991/aisr.k.200424.032.

Zhang, G.C., Huang, H., Qin, H.D., Wan, L., Li, Y.M., Cao, J., Su, Y.M., 2018. A novel adaptive second order sliding mode path following control for a portable AUV. Ocean Eng. 151, 82–92. http://dx.doi.org/10.1016/j.oceaneng.2017.12.054.

Junhe Wan was born in YiChun, HeiLongJiang, China in 1982. She received her Ph.D. degree in intelligent information and communication system from Ocean University of China in 2020. She is currently a junior research fellow in Institute of Oceanographic Instrumentation, Qilu University of Technology (Shandong Academy of Sciences). Her research interest includes motion control based on fractional-order PID and fractional-order active reject disturbance control for AUV.

Yi Zheng was born in RuShan, ShanDong, China in 1978. He completed his Ph.D. degree from Beijing Institute of Technology, Beijing, China, in 2006. He is currently a senior research fellow and the Director of Institute of Oceanographic Instrumentation, Shandong Academy of Sciences. His research areas lie in ocean acoustic and Oceanographic instrumentation.

Yanping Li, Ph.D. candidate in School of Electrical and Information Engineering, Tianjin University, is committed to the research of Co-prime Spectral Analysis, and participated in the project "Research on broadband spectrum sensing theory and technology based on mutual prime sampling" sponsored by NSFC . Qingdao cloud service platform information service expert, "World Bank GEF Jiangxi project" technical director, studied in Jiangsu Donghua postdoctoral innovation practice base, China Academy of Engineering Physics Information Science, control science and engineering special class.

Lv Bin was born in Qingdao, Shandong, China in 1980. He received his MA.Eng degree in project management from Ocean University of China in 2011. He is currently an associate professor in Institute of Oceanographic Instrumentation, Shandong Academy of Sciences. His research interest lies in the deep sea detection technology and AUV intelligent control.

Yinglong Wang received the Ph.D. degree in Communication and Information Systems from Shandong University in 2005. He is currently a senior research fellow, the secretary of Party committee of Qilu University of Technology (Shandong Academy of Sciences), and chief scientist of Natural Key Research and Development Program of China. Currently, his research interests include artificial intelligence, high-performance computing, and cloud computing.